PERGAMON

International Journal of Heat and Mass Transfer 43 (2000) 3073–3086

International Journal of HEAT and MASS TRANSFER

www.elsevier.com/locate/ijhmt

The effect of a surfactant monolayer on the temperature field of a water surface undergoing evaporation

J.R. Saylor [a,*], G.B. Smith [a], K.A. Flack [b]

[a] *Naval Research Laboratory, Washington, DC 20375, USA*
[b] *United States Naval Academy, Annapolis, MD 21402, USA*

Received 16 February 1999; received in revised form 5 November 1999

Abstract

The surface temperature field of a body of water undergoing evaporation was measured using infrared imaging techniques, demonstrating for the first time the effect of surfactant monolayers on the spatial structure of this field. Measurements were obtained from a water surface which was covered with a monolayer of the surfactant oleyl alcohol, and also from a surface which was free of surfactants. The oleyl alcohol and surfactant-free experiments were compared at equivalent heat fluxes. The presence of surfactants increased the characteristic length scale of the surface temperature field. This conclusion is supported by both visual observation of the infrared imagery and spatial Fourier transforms of the temperature fields. The presence of the surfactant monolayer had a small effect on the root mean square of the temperature field but significantly affected the skewness, creating a more positively skewed probability density function for the surfactant covered field. These observations were found to hold when comparison between the clean and surfactant case was made at heat fluxes varying by a factor of ~11.

Keywords: Evaporation; Convection; Surfactants; IR imagery; Remote sensing

1. Introduction

The process of evaporation engenders a complicated coupling between the fluids on both sides of a gas/liquid interface. Evaporation at such an interface results in a cooling of the liquid near the surface, increasing its density and causing the liquid portion of the system to become unstable, resulting in natural convection. Under typical conditions, this natural convection is turbulent, and the resulting temperature and velocity fields are complex. On the gas side of the interface, a similar situation can occur if the density of the vapor created by the evaporating liquid is different from the density of the gas initially residing above the liquid. This causes changes in the density profile and can initiate natural convection in the gas, or modify any existing convection. Evaporative cooling of the liquid surface results in temperature changes which in turn alter thermal transport from the gas to the liquid (and similarly on the liquid side from the bulk liquid to the surface liquid). All these natural convection processes are driven by, or related to, evaporation and are referred to as 'evaporative convection' [1]. Additional complexity is added to the evaporative convection problem if forced convection exists in either the gas or liquid phases. Finally, the presence of a surfactant monolayer at the gas/liquid interface can profoundly

* Corresponding author.

0017-9310/00/$ - see front matter
PII: S0017-9310(99)00356-7

Nomenclature

c	surface concentration
E	elasticity
Ma	Marangoni number, Eq. (2)
p	surface pressure
q''	heat flux
S	surface tension
t	time
T	surface temperature
$\bar{T}$	average surface temperature
T_b	bulk water temperature
T_{air}	air temperature

Greek symbols

γ	skewness coefficient of surface temperature, Eq. (1)
ϕ	relative humidity
σ	rms of surface temperature

affect the system by damping fluid motion and also by suppressing evaporation.

Evaporation from a water surface has important implications in applications such as oceanography and limnology; it affects weather and is an important unknown in climatological modeling. Evaporative cooling at the air/water interface causes spatial and temporal variations of the water surface temperature. These spatial and temporal variations in surface temperature can be remotely sensed using infrared cameras and radiometers. This suggests the possibility of obtaining remotely sensed information on evaporative processes as well as information on the fluid dynamics occurring near the air/water interface. One of the long-term goals of research of the type presented herein is the extraction of subsurface hydrodynamics from remotely sensed imagery of the ocean surface, such as remote measurements of the surface temperature field. While knowledge of the surface temperature field alone cannot provide a complete understanding of subsurface hydrodynamics, such knowledge may provide insight into what occurs beneath the water surface.

There are several poorly understood aspects of the evaporative convection problem which must be investigated before knowledge of the surface temperature field can provide information about subsurface hydrodynamics. One of these aspects is the effect of surfactant monolayers on the surface temperature field. The extent and manner by which surfactants modify the surface temperature field must be known so that their effect is not confused with signatures due to other phenomena occurring near the air/water interface. It is the goal of this work, then, to isolate the effect that surfactant monolayers have on evaporative convection and the surface temperature field. The successful completion of this task will represent a step toward obtaining subsurface hydrodynamics from remotely sensed infrared imagery of the water surface.

Surfactant monolayers have typically been studied within the context of evaporation suppression. Since the seminal work of Rideal [2], there have been numerous studies of the suppression of evaporation by surfactant monolayers, as well as on the specific chemical and physical attributes which are responsible for evaporation suppression. Summaries of this aspect of surfactant monolayers can be found in reviews due to La Mer [3] and Barnes [4]. The work presented here does not address this aspect of surfactant monolayers, but rather focuses on the hydrodynamic damping which surfactants introduce to the air/water interface, and how this damping affects the surface temperature field. In the current work, a surfactant which does not suppress evaporation was purposely selected so that the hydrodynamic damping characteristics of surfactant monolayers and their effect on the surface temperature field could be investigated, independent of the dynamics of evaporation suppression. A review of those studies which address this specific aspect of surfactants is now presented.

Navon and Fenn [5,6], while not explicitly noting the role of surfactants on surface temperature, conducted experiments demonstrating that the hydrodynamic damping properties of surfactants are important, beyond their ability to suppress evaporation. In a pair of papers, they demonstrated that the reduction in the heat transfer from a body of water, caused by an evaporation-impeding surfactant, was larger than that which could be accounted for by evaporation suppression alone. They concluded that an inhibition of natural convection in the water, caused by the hydrodynamic damping properties of the surfactant, was the reason for this.

Ewing and McAlister [7] utilized an infrared radiometer to measure the surface temperature of a body of water undergoing evaporation. They demonstrated that a reduction in the surface temperature occurred when evaporation was enhanced by an imposed air velocity. However, no results concerning the role of surfactants on their measurements were reported.

Jarvis [8] appears to be the first author to recognize how surfactants which do not affect evaporation influence the surface temperature of an air/water interface.

Jarvis [8] showed that the presence of a monolayer of oleic acid, which does not impede evaporation [9], affects both the average and the fluctuating component of the surface temperature time trace obtained at a point, and concluded that the influence of a monolayer on convection in the water, has an important effect on the surface temperature, independent from its effect on evaporation.

Jarvis [8] obtained surface temperature time traces at two different gas flow rates, and demonstrated that when the gas flow rate was small, the addition of an oleic acid monolayer had no effect on the surface temperature. In contrast, at a high gas flow rate (and presumably a higher heat flux), the addition of an oleic acid monolayer increased the magnitude of the surface temperature fluctuations.

Katsaros and Garrett [10] performed experiments under conditions similar to those of Jarvis [8]. Oleyl alcohol, which the authors showed did not impede evaporation, was used as the surfactant. Experiments were conducted with no air flow, as well as with an air flow of 1 m/s, which increased the heat flux. The authors observed no change in the rms of the surface temperature σ, upon addition of the surfactant monolayer, when there was no air flow. With a 1 m/s air flow, however, the addition of oleyl alcohol increased σ by a factor of 2 to 3. These results agree with those of Jarvis [8], if one considers the low gas flow case of Jarvis [8] to be analogous to the zero wind case of Katsaros and Garrett [10].

Katsaros and Garrett [10] increased the heat flux yet further by repeating their experiments with the bulk water temperature elevated by $\sim 8^{\circ}C$ above the air temperature. In these experiments, they found that addition of oleyl alcohol had no effect on the surface temperature and concluded that when the heat flux gets sufficiently high, buoyancy forces in the liquid become large enough to render any surface effects negligible.

The goal of the experiments presented here is to ascertain the effect of a surfactant monolayer, which does not impede evaporation, on the surface temperature field, and to investigate this effect at different heat fluxes. Such experiments extend the work of the aforementioned studies in several ways. First, in all of the studies described above, measurements of surface temperature were obtained at a point, providing time traces. Such time traces do not provide information concerning the spatial structure of the surface temperature field, an important aspect of the problem from the remote sensing perspective. Measurements of the surface temperature field reveal how the structures present in this field are affected by the presence of a monolayer, and how this effect varies with heat flux.

Another important aspect of the experiments presented here is that the heat flux is varied without the use of forced convection. In some of the work cited above, the heat flux was varied by increasing the flow of a gas above the water surface. This complicates interpretation of the results since changes in the measured surface temperature may be due to velocity and pressure fluctuations caused by the gas flow, or they may be due to a change in the subsurface hydrodynamics caused by the increased heat flux. In the experiments presented here, this complication is avoided by using the water temperature as a tool for varying the heat flux.

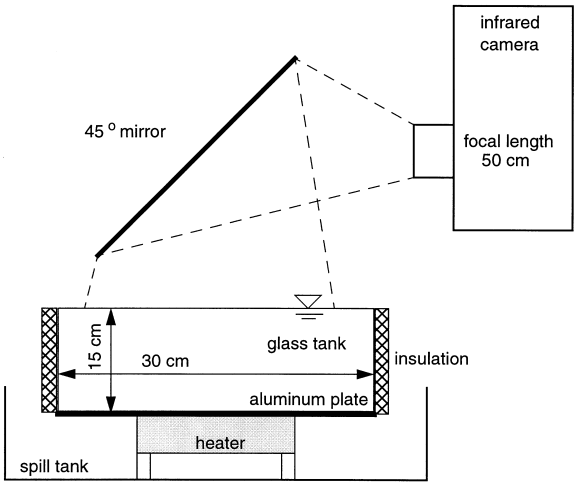

Fig. 1. Schematic illustration of the experimental setup used to obtain temperature fields from the surface of a body of water during evaporation.

Finally, the experiments presented here provide higher resolution measurements. The time traces presented in the work of Jarvis [8] and Katsaros and Garrett [10] show turbulent behavior. Yet in both studies, a rather large temperature sensor was used. Jarvis [8] employed a thermistor which was housed in a glass probe 1 cm long and 0.2 cm in diameter. Katsaros and Garrett [10] utilized a resistance film probe 1.2 mm long and 15 μm in diameter. Since the thermal boundary layer is expected to be about 1 mm in thickness, it is possible that measurements obtained using a probe of this size may have missed small scale turbulent fluctuations. Furthermore, in both of the aforementioned studies, measurements were obtained at a location 2 mm beneath the surface. This distance is significantly removed from the surface where evaporation acts to change the surface temperature field and, as a result, small scale structures generated by evaporation may have been blurred before they were transmitted via conduction to a location 2 mm beneath the surface. Imagery obtained from infrared cameras can gather radiation evolving from a surface layer only 25 μm

thick and would therefore represent a significant improvement over existing studies.

In this paper, evaporation from the free surface of a small body of water is considered. The surface temperature field is measured using an infrared camera on a surface which is nominally free of a surfactant monolayer, as well as one coated with a monolayer of oleyl alcohol. Experiments were conducted for situations where the air and water temperature are essentially the same, as well as for cases where the water temperature is elevated above that of the air. These experiments reveal changes in the surface temperature field caused by (i) the presence of a monolayer, and (ii) a change in heat flux.

2. Experimental method

2.1. Setup

An illustration of the experimental setup used in these experiments is presented in Fig. 1. Water was contained in a glass tank, 30 cm × 30 cm on a side and 15 cm deep. The tank was filled to the rim during all experiments. The water height changed negligibly during the course of an experiment. The tank was constructed of glass and was sealed using RTV silicone rubber which cured for several days before any experiments were conducted. The tank was then cleaned with methanol, thoroughly washed with copious amounts of deionized water, and filled with deionized water for several more days in order to leach out any surface active material in either the cured RTV or on the glass walls of the tank.

Forced convection was absent on the water side of the interface. On the air side of the interface, natural convection, combined with any background room air motion was responsible for fluid motion. Heat transfer across the air/water interface was due to both evaporative cooling at the water surface and to differences between the bulk air and water temperatures. The body of air was large, and introduction of water vapor by evaporation from the tank did not change the density or relative humidity of the air, for the experiments presented here.

The water used in all experiments was obtained from a deionization system (Milli-Q UV Plus) consisting of a single distillation unit, followed by a millipore filter and a UV filter. After deionization, the only objects the water came into contact with were a nalgene carboy, Teflon tubing, and the tank itself.

The sides of the tank were insulated using 2.5 cm thick polystyrene foam having an R value of 5. The bottom of the tank was in contact with a heater which also served as the tank support. Prior to the high flux experiments, this heater was used to elevate the bulk temperature of the water. During the low flux experiments, the heater was not used. In order to reduce the thermal stress on the glass floor of the tank during heating, an aluminum plate was glued to the bottom of the tank, leaving a small air space between the aluminum plate and the outer surface of the bottom glass panel.

Deionized water was stored in a large nalgene carboy, connected to the water tank by a Teflon tube which entered the tank through an orifice in the tank floor. Flow to the tank was controlled by a Teflon valve. As a precaution against unwanted surfactant contamination, water was taken from the bottom of the carboy, far from the surface where surfactants tend to collect.

Measurements of the heat flux were obtained by calorimetry. The bulk water temperature was measured using a mercury in glass thermometer, having a resolution of 0.1°C, and the rate of decrease in temperature, $\mathrm{d}T_\mathrm{b}/\mathrm{d}t$ was used, along with the density, specific heat and water volume, to compute the total heat loss from the water. The heat loss was then corrected for heat transfer through the insulated tank walls and floor, and this corrected value was divided by the surface area of the water to give the heat flux q''. As indicated in Table 1, the heat flux was $q'' = 407 \pm 5$ W/m^2 for the high heat flux cases, and $q'' = 38 \pm 11$ W/m^2 for the low heat flux cases.

Oleyl alcohol (white, Hormel Institute) was used for all of the surfactant runs. A stock solution of oleyl alcohol in HPLC grade heptane was prepared and deposited on the water surface using a micrometer syringe. The solution was applied in ~10 μl increments. These drops formed small liquid lenses which left an oleyl alcohol monolayer as the heptane evaporated. In all surfactant runs, the oleyl alcohol concentration was $c = 0.11$ μg/cm^2. Care was taken to properly seal the glass container containing the surfactant solution, to insure that the concentration did not change via evaporation of heptane.

Infrared images of the water surface were obtained using a Raytheon-Amber AE4256 CCD camera containing a 256 × 254 InSb array. The camera is liquid nitrogen cooled and exhibits a noise level equivalent to approximately 25 mK in measured temperature at each pixel. A mirror angled at 45° was used to direct the image of the water surface onto the camera detector. The imaged footprint was about 16 cm on a side (this varied somewhat from experiment-to-experiment, as noted in Section 3), centered within the tank. The only optics used were a 50 cm focal length lens and a bandpass filter which passed wavelengths between 3 and 5 μm. The detector itself is sensitive to wavelengths between 2 and 5 μm.

Table 1
Environmental conditions for each of the four cases considered

Case	$\bar{T}$ (°C)	T_b (°C)	$\bar{T} - T_b$	T_{air}	ϕ	q'' (W/m^2)
High flux, clean	32.6	32.7	−0.1	20.3	0.49	407
High flux, surfactant	34.7	36.0	−1.3	19.1	0.67	407
Low flux, clean	16.9	17.9	−1.0	19.0	0.54	38
Low flux, surfactant	16.4	17.5	−1.1	19.4	0.53	38

2.2. Calibration

Two calibration steps were employed to enable conversion of pixel intensity to temperature. The first step involved a nonuniformity correction, where the gain and offset of each pixel was individually adjusted. This corrected for any variation in performance of individual pixels, insuring that when a uniform temperature surface was imaged, the output was also uniform. This correction was performed at two temperatures and the gains and offsets were optimized by the camera controller to yield the most uniform image for the temperature range under consideration. The uniform temperature surface which was utilized during the nonuniformity correction was a digital black body (Electro Optical Industries, model LDS100-04 controller and 2498B black body) capable of imposing a controlled temperature across the face of a 10.2 cm square surface. The emissivity of the surface of the black body was 0.99 ± 0.01. The black body temperature was defined by the user and could be set to any value between -5 and $+95$°C to an accuracy of ± 0.015°C.

Once the nonuniformity correction was complete, the gain and offset of the camera amplifier was adjusted to provide an appropriate dynamic range for the temperature range being imaged. A second calibration was then performed to enable conversion of the measured pixel intensities to temperatures. This was achieved by imaging the black body at two different temperatures within the temperature range of interest, and storing those images. These images were subsequently used to provide the pixel intensity versus temperature calibration curve. A linear fit was used to do this. The actual relationship between photon counts and temperature is not linear, and is proportional to the fourth power of temperature. However, for the experiments reported here, the range in temperature over which the calibration was performed varied from 1.5 to 4.5°C, and a linear fit resulted in an error which was less than 0.25% in all cases.

Finally, a length scale calibration was performed to correlate the relationship between the size of structures in the imagery and their actual size in physical space. This was accomplished by imaging a ruler at the conclusion of each experiment, from which a length-per-pixel value was computed.

The camera had 12-bit intensity resolution, giving a range in pixel intensities varying from 0 to 4095. In any given image, a number of pixels gave erroneous responses, resulting in either a very high or a very low value. These 'bad pixels' were small in number and had a negligible effect on the image appearance or average surface temperature. However, inclusion of these pixels did affect the higher order moments σ and γ. To eliminate this error, these pixels were identified and later set to the average value for that frame, prior to computation of any statistical or spectral quantities. Bad pixels were identified as those having a value of 0, 1, 4094 or 4095. The gain of the camera amplifier was set so that the maximum and minimum temperatures viewed did not result in intensities close to these extreme values, obviating the possibility that pixels having these four values might be legitimate pixels. This point was checked by purposely identifying an even larger range of intensities as bad pixels, to see if the computed moments changed. This was observed not to be the case, indicating that the tails of the true image pdf did not extend into the range [0, 1] and [4094, 4095], further justifying the elimination of these pixels.

2.3. Procedure

Prior to all experiments, the tank was filled and allowed to slowly overflow for at least an hour prior to data acquisition. The purpose of the overflow was to drain off any contaminating monolayers existing on the water surface. Coincident with this overflow process was a sparging process, wherein a glass frit was introduced into the water bulk and nitrogen gas was bubbled through the water. The purpose of sparging was to accumulate any surfactants which existed in the bulk water onto the free surface, where they spilled over the tank edge into the underlying catch basin. Upon completion of this surface cleaning procedure a glass rod was used to swipe the water surface, pushing any remaining surfactant film over the tank edge. The glass rod was washed with methanol and then deionized water, prior to being used to swipe the water

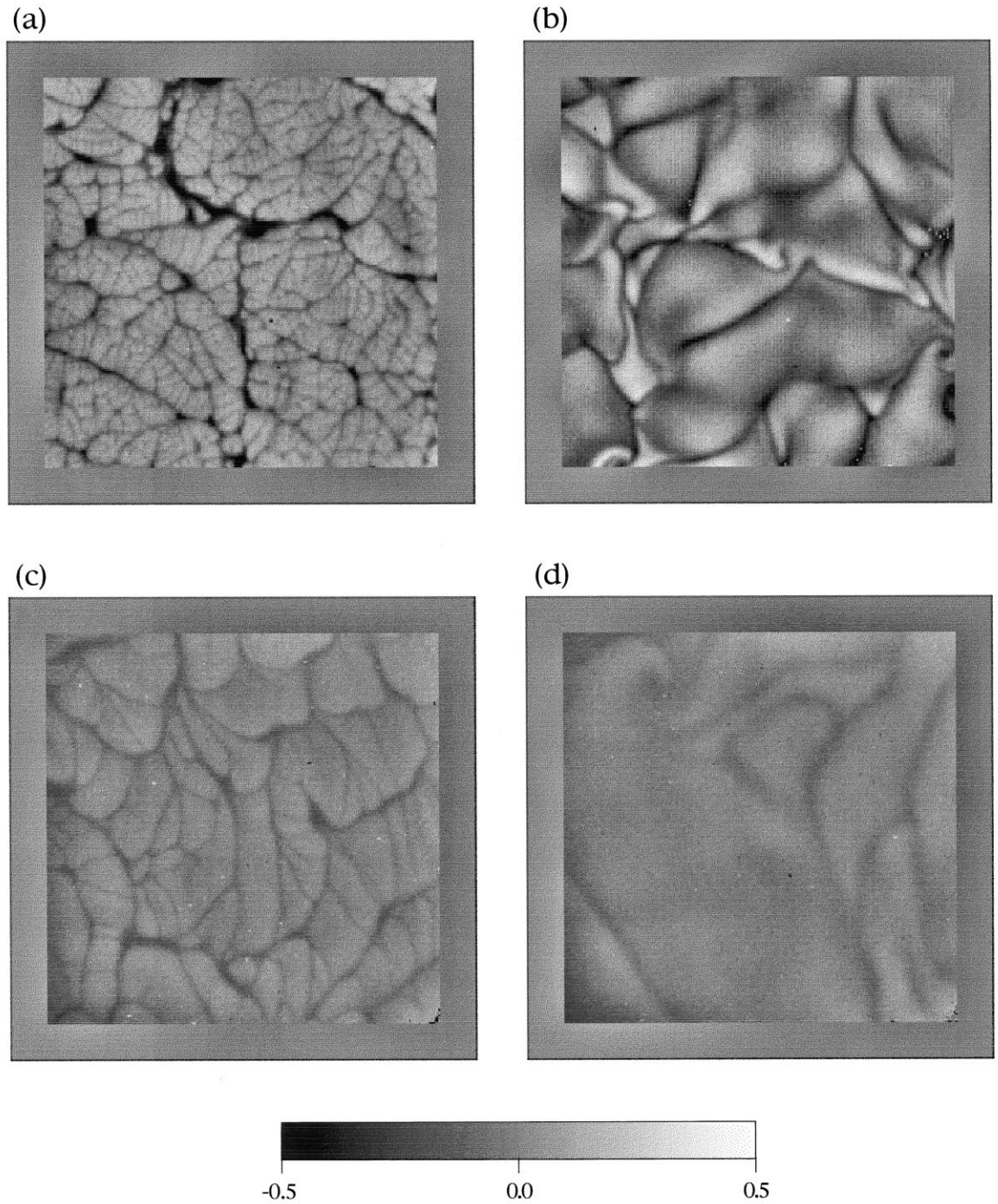

Fig. 2. Sample temperature fields at the four experimental conditions considered. (a) High heat flux, $c = 0$ μg/cm^2; (b) high heat flux, $c = 0.11$ μg/cm^2; (c) low heat flux, $c = 0$ μg/cm^2; (d) low heat flux, $c = 0.11$ μg/cm^2. The width of images (a)–(d), in physical space, is 17.1, 15.7, 16.1 and 16.1 cm, respectively.

surface. During the low heat flux runs, data acquisition was initiated shortly after this final swiping process. During experiments without surfactant monolayers, this swiping process was repeated in between image acquisitions, to remove any surfactant contamination which might have accumulated on the water surface during the run.

The process was slightly different for the high heat flux runs. In this case, the heater was turned on during the process of bubble sparging and tank overflow. The tank overflow was sufficiently slow that the water could be heated even while room temperature water was being introduced. When the water reached the desired temperature, the heater was turned off. At this point in time, the heater was still hot and it was assumed that buoyant plumes of warm fluid were still being formed at the floor of the tank. Since the objective of the experiments was to measure the temperature field for evaporatively driven convection, a waiting period was introduced to allow the heater plate to cool. A thermocouple was inserted into the air space between the aluminum plate and the glass tank floor, and data acquisition was not initiated until this temperature dropped to the bulk water temperature. In this way, the possibility of convective motions originating from anywhere other than the water surface, was eliminated.

3. Results

Experiments were conducted at a high and a low heat flux, with and without a surfactant monolayer, resulting in four experimental conditions: (a) high flux, clean, (b) high flux, surfactant, (c) low flux, clean, and (d) low flux, surfactant. The low heat flux case refers to conditions where the water was initially at room temperature. The heat flux in this case was 38 W/m^2. The high flux case refers to cases where the water temperature was elevated. The value for the heat flux in these runs was 407 W/m^2, as indicated in Table 1.

Fig. 2 presents sample temperature fields corresponding to each of these four experimental conditions. In all four images, the average temperature has been subtracted, so that white represents temperatures above the average, and black represents temperatures below the average. These images have also been high pass filtered to eliminate a large scale spatial variation in the mean intensity. This variation was most likely due to an imperfect nonuniformity correction during the camera calibration procedure (Section 2.2), and is further discussed later in this section.

The most apparent difference between the temperature fields of clean and surfactant covered water surfaces, displayed in Fig. 2, is the difference in the spatial dimension of the structures present. The clean

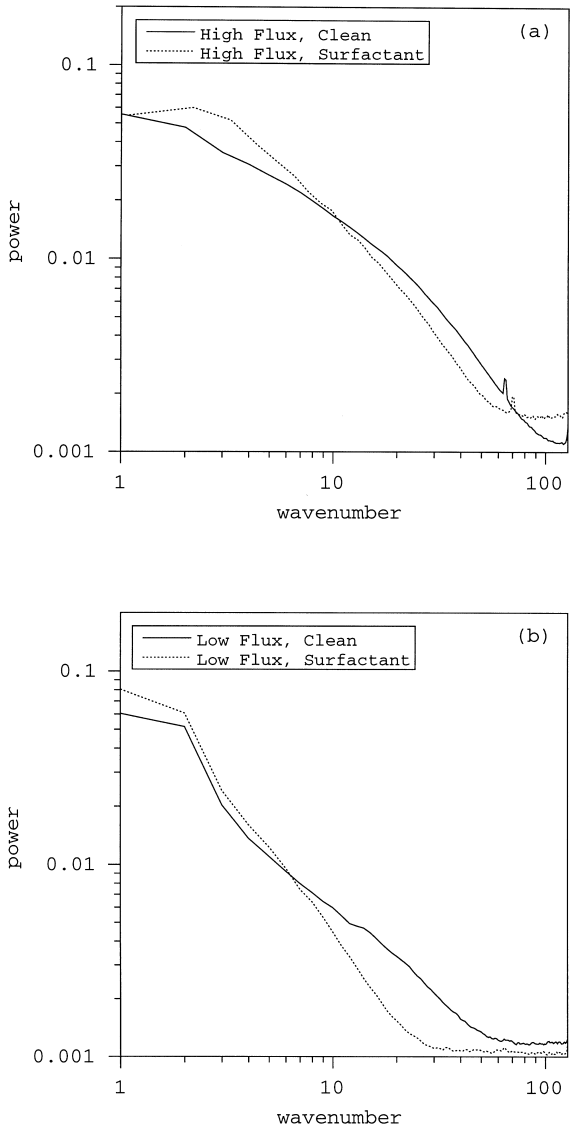

Fig. 3. The x-direction Fourier transform for the four experimental conditions considered. Ensemble average obtained over 119 frames of data. (a) High heat flux cases; (b) low heat flux cases. The wavenumber indicated in the abscissa is defined as $256/\lambda$ where λ is measured in pixels.

images have considerable small scale structure, while the surfactant covered imagery displays an absence of small scale structure. As indicated in the caption for Fig. 2, there is a small variation in the physical dimensions from image to image. This was due to slight changes in the camera-to-water distance from experiment-to-experiment. The difference between frames (a) and (b) is 9%. This difference was compensated for prior to computing spatial quantities. The image size

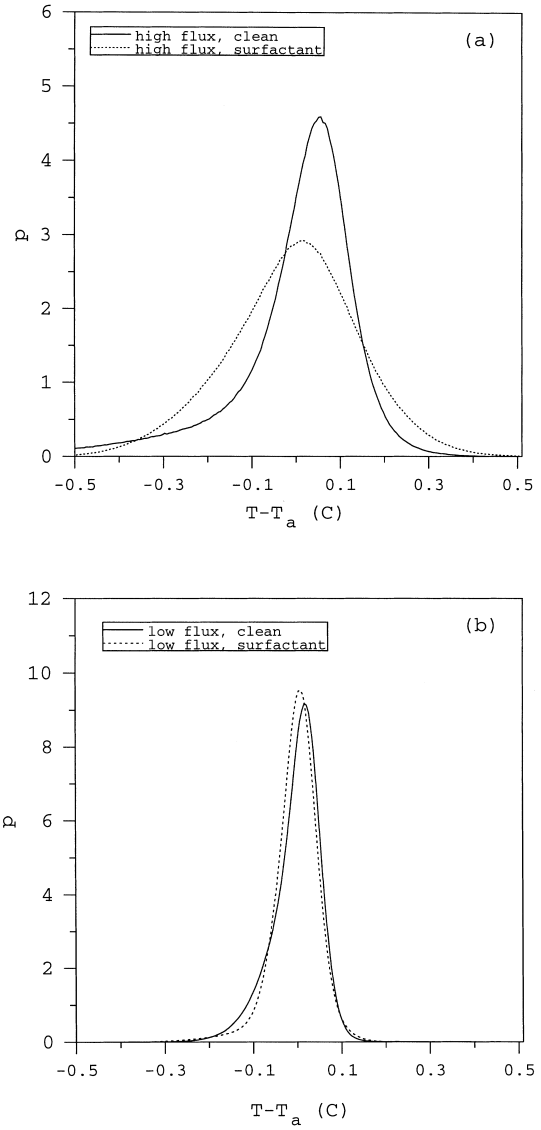

Fig. 4. Probability density function of $T-\bar{T}$ for each of the four experimental conditions. The three lowest spatial frequencies are filtered out of the images prior to obtaining these pdfs. Each pdf is an ensemble average obtained using 119 frames of data. (a) High heat flux cases; (b) low heat flux cases.

was exactly the same for images (c) and (d). In addition to the difference in spatial scale, there was also a significant difference in the speed at which the structures in the image evolved. For both heat fluxes, the temporal rate of change was much higher in the clean run than in the surfactant run.

Quantification of the degree of small scale structure in these images is presented in Fig. 3, where spatial Fourier transforms are presented. These are x-direction Fourier transforms, obtained by ensemble averaging the transform of each row of each of the 119 images. The x-direction Fourier transform is representative of the image, due to the high degree of radial symmetry displayed by the two-dimensional spatial Fourier transforms (not shown). For the high flux case, the clean spectrum is larger than the surfactant spectrum between the wavenumbers, roughly, 10 and 70. For the low flux case, the clean spectrum is greater than the surfactant spectrum for wavenumbers greater than roughly 6. At low wavenumbers, the surfactant spectrum is larger than the clean spectrum, for both heat fluxes, confirming the visual observation that there is more large scale structure in the surfactant images. It seems, then, that the small scale structure which is apparent in the clean imagery corresponds to structures having wavenumbers greater than 10 for the high flux case, and 6 for the low flux case, corresponding to wavelengths of 26 and 43 pixels, respectively. Differences between the spectra at very high wavenumbers represent spatial variations over a very small number of pixels and is attributed to high frequency noise.

Table 2
Statistics for each of the four cases considered (the rms σ and skewness γ are computed for the surface temperature T)

Case	σ	γ
High flux, clean	0.14	−1.72
High flux, surfactant	0.13	−0.20
Low flux, clean	0.04	−1.04
Low flux, surfactant	0.03	−0.33

The spatial Fourier transforms presented in Fig. 3(a) and (b) have been corrected to account for the difference between the physical image size in Fig. 2(a) and (b), discussed earlier. Hence, the comparison between clean and surfactant spatial Fourier transform pairs can be made without rescaling wavenumbers.

In addition to creating a variation in the spatial scale of the thermal structures in the temperature field, the presence of a surfactant monolayer affected the statistical distribution of the temperature fields. Fig. 4 presents probability density functions (pdfs) for the four experimental conditions considered. These plots demonstrate that the presence of a surfactant significantly affects the shape of the pdf. Table 2 catalogs the rms σ and the skewness γ for these distributions, quantifying the breadth of the distributions and the degree of asymmetry. Here, we define the skewness as

$$\gamma = \frac{\overline{(T-\bar{T})^3}}{\sigma^3}. \tag{1}$$

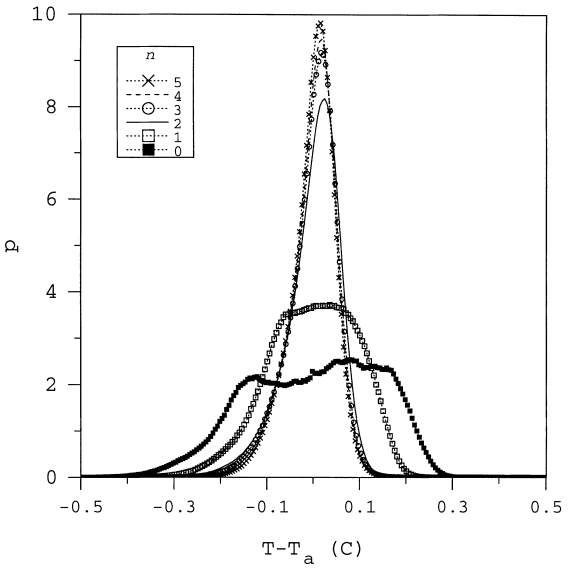

Fig. 5. Probability density functions for the low heat flux, clean case. Each plot is a pdf, for the same data set, with a different set of wavenumbers filtered from the image prior to pdf computation. The lowest $[-n, n]$ wavenumbers were removed in each plot, with n varying from 0 to 5. Each pdf is an ensemble average obtained from 119 frames of data.

As was described earlier in this section, the original temperature fields exhibited a large scale spatial variation in the mean intensity that is thought to be due to an imperfect nonuniformity correction during the infrared camera calibration. This error was corrected by first performing a spatial Fourier transform of each image, setting the lowest three wavenumbers to zero (wavenumbers $[-3, 3]$) and then reconstructing the image via the inverse Fourier transform. The pdfs presented in this paper were all obtained from images corrected in the aforementioned fashion. The number of wavenumbers n which were set to zero was chosen with the goal of correcting the low frequency intensity variation while throwing away the smallest amount of information possible. In Fig. 5, the pdf for the low heat flux, clean case (the case where the image nonuniformity appeared to be the worst) is replotted for $n = [0, 5]$. This figure shows that for $n = 0$ or 1, the pdf displays anomalous behavior. For $n \geq 3$, the pdf appears to approach an asymptotic form. Accordingly, $n = 3$ was chosen as the value which eliminated the least amount of information, while providing a pdf which is close to the asymptotic form. It is noted that the Fourier transforms presented in Fig. 3 were obtained from the uncorrected images.

4. Discussion

The main result of this work is that small scale structures in the surface temperature field are suppressed by the presence of a surfactant monolayer. This conclusion is supported by Figs. 2 and 3. To the authors' knowledge, this effect on the two-dimensional temperature field has not been reported previously.

Although this result is new, the fact that surfactants impart a surface viscosity to an air/water interface makes the suppression of small scale structures in the temperature field somewhat predictable. It is well known that an increase in the bulk viscosity in single phase turbulence will result in an increase in the size of the smallest eddies present in the flow. It should also be expected to be the case, therefore, that the increase in surface viscosity caused by the introduction of a surfactant monolayer will reduce the amount of small scale turbulent structure at a free surface. What was unexpected, however, was the degree to which these structures were damped. Comparing the clean and surfactant images of the high flux case (Fig. 2(a) and (b)), the characteristic distance between the dark lines (which indicate falling sheets of cool liquid), is quite large for the surfactant case. In Fig. 2(b), separations are on the order of 10 or more pixels, while for the clean case (Fig. 2(a)), these dark lines are very close together, approaching the spatial resolution of the camera.

While the differences between Fig. 2(a) and (b) are obvious and present a graphic demonstration of the effect of surfactant monolayers on the surface temperature field, line sections through these very same images are more difficult to interpret. Fig. 6 presents horizontal line sections through the centers of Fig. 2(a) and (b). While differences in scale size are obvious in the two-dimensional images, differences in the line sections are much less apparent. This is an important point for two reasons. First, in the work of Jarvis [8], two-dimensional images were not obtained and only time traces were reported. Statistics were not computed from these time traces. Hence, the role of surfactant monolayers was inferred from the qualitative appearance of the time traces which did not differ in the clean and surfactant cases, for some of the conditions. The lack of an obvious difference between the line sections presented in Fig. 6 suggests that, in the work of Jarvis [8], the temperature field may actually have been very different, even when the time traces appeared to be similar (this argument assumes that the time traces of surface temperature obtained at a point behave similarly to the line sections presented in Fig. 6).

The aforementioned observation is also important from the perspective of remote sensing. For example, the use of various remote sensing techniques for the detection of surfactant slicks has been well documented

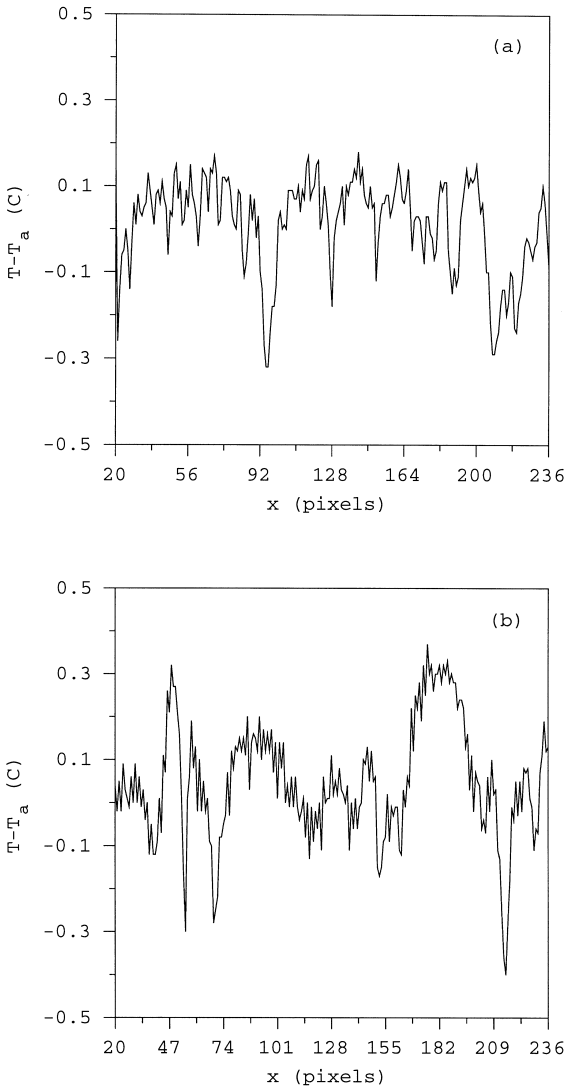

Fig. 6. Plot of $T-\bar{T}$, obtained from horizontal line sections through the center of Fig. 2(a) and (b): (a) high flux, clean, (b) high flux, surfactant.

by, for example, Lombardini et al. [11], Milgram et al. [12], and Peltzer et al. [13]. However, these methods rely on the ability of surfactants to damp water waves. That is, the presence of a surfactant slick is determined from a lack of surface roughness in the slick area. Under conditions where there are no waves, due to calm wind conditions, the aforementioned methods will not work. The current results suggest that infrared detectors may allow one to ascertain the presence of surfactant monolayers under these conditions, where methods based on surface roughness fail. However, the lack of obvious differences between the plots presented

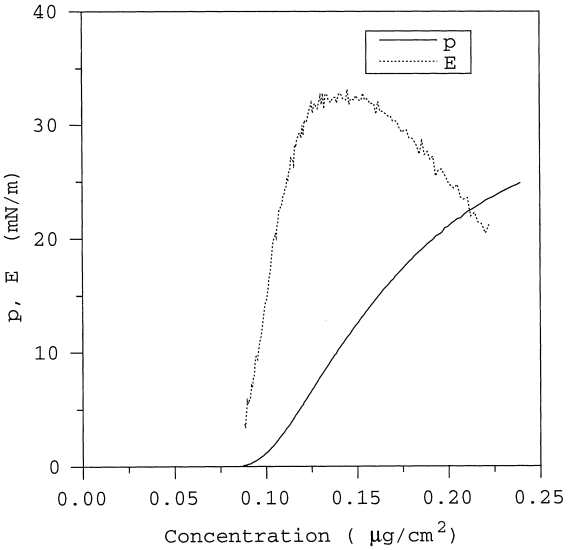

Fig. 7. Plot of surface pressure p and elasticity E, as a function of surface concentration, for oleyl alcohol. Data due to Barger [14].

in Fig. 6 suggests that imagery is preferred for such a task and that time traces obtained from radiometers, for example, would not serve adequately in this regard. An additional point to note is that while spatial Fourier transforms were successfully used to quantify differences in spatial scale between clean and surfactant cases, more sophisticated methods can be employed to classify the images. Alternative methods, such as wavelet analysis or Karhunen–Loeve decomposition, for example, may be even more effective in quantifying the differences observed in Fig. 2(a) and (b).

The results presented here demonstrate that a very small quantity of surfactant will result in significant damping of small scale structures in the surface temperature field. While the surfactant experiments presented in this paper were conducted at a surface concentration of $c = 0.11$ μg/cm^2, data from other experiments, not presented here, were conducted at a concentration of $c = 0.011$ μg/cm^2, a factor of 10 smaller, and showed temperature fields qualitatively the same as the surfactant cases presented here. To put these concentrations in perspective, plots of surface pressure p and elasticity E [14], are presented as a function of surface concentration in Fig. 7. This figure shows that E and p are significant for an oleyl alcohol monolayer at $c = 0.11$ μg/cm^2 but when the concentration is reduced by a factor of 10, p and E fall into the noise floor of the measurement. Hence, even when c becomes so small that $E \rightarrow 0$, the damping of surface structures can still be observed.

Additional evidence in support of this conclusion was provided by an accidental observation which

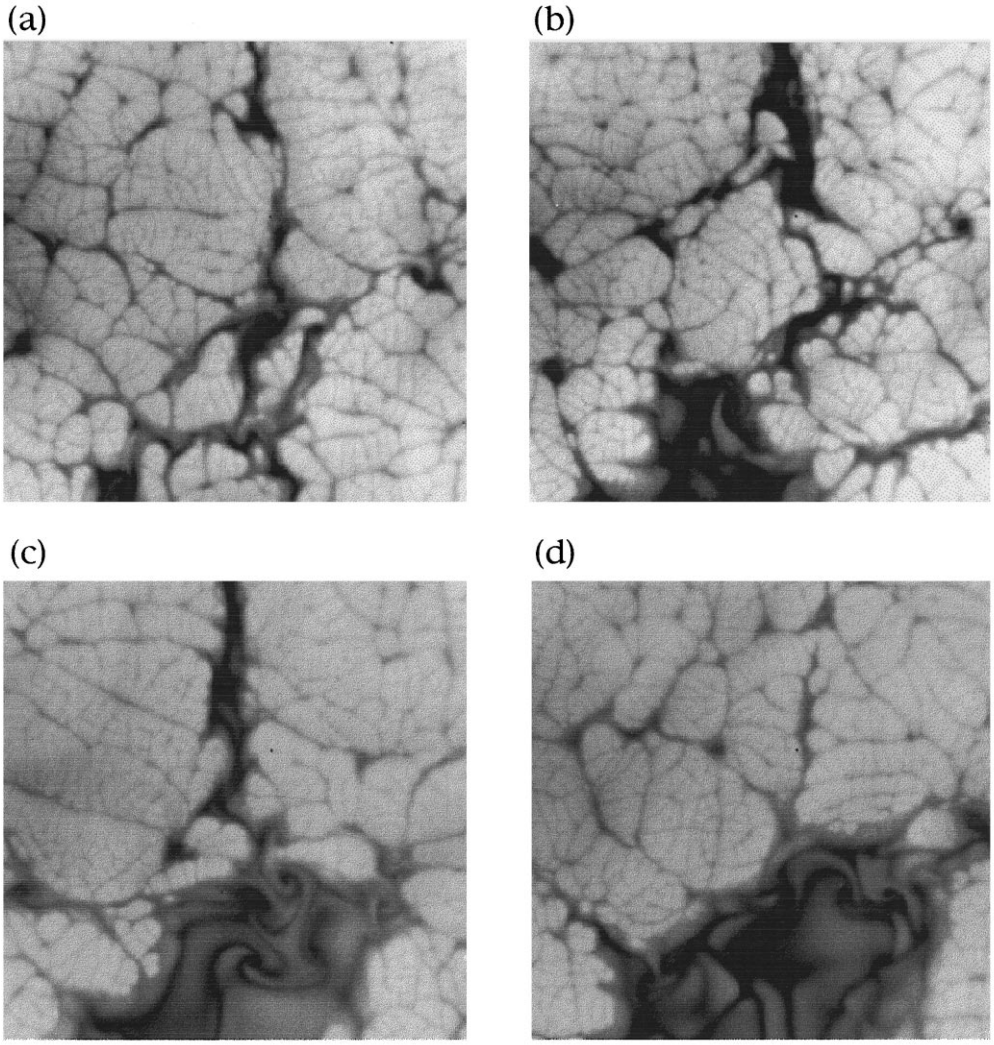

Fig. 8. Sequence of four infrared images illustrating the spread of a contaminant surfactant on the water surface. The time between each image is 25 s.

occurred in some of the experiments. The experimental procedure necessitated using the same tank of water for several hours. The tank was overflowed periodically, and the free surface was swiped with a glass rod in between experiments so as to maintain the cleanliness of the free surface. However, in spite of these precautions, after several hours the infrared imagery obtained in some of the experiments revealed what is assumed to be contamination by an adventitious surfactant. A series of infrared images is presented in Fig. 8 illustrating this phenomena. It is readily apparent in these images that the thermal structure in the lower portion of each frame is being modified. In this region, the scale size is larger and the temperature is lower. Independent measurements of the surface tension in this region were not made, and so it can not be stated with certainty that this structure was caused by an encroaching surfactant film. Nevertheless, the similarity of this structure with the general appearance of Fig. 2(b) (where a surfactant monolayer was purposely introduced), is undeniable. The careful procedures taken to ensure surface cleanliness suggests that the quantity of surfactant causing the behavior observed in Fig. 8 is quite small, furthering the conclusion that the transition between 'clean' behavior and surfactant-dominated behavior occurs at a very low surface concentration.

Recent work due to Handler et al. [15] lends further credence to this point. In this investigation, direct numerical simulations of a vortex pair impinging on a

free surface from below, are presented. Simulations were conducted at several values of the Marangoni number Ma, defined as

$$Ma = -\frac{\partial S}{\partial c}\frac{c}{S}, \tag{2}$$

where S is the surface tension at a surfactant concentration c. These simulations showed that, for $Ma > 10^{-2}$, the dynamics of the subsurface hydrodynamics are virtually identical to those of a surface having a no-slip boundary condition (viz. a solid wall), and behavior similar to a completely clean surface is not observed until $Ma < 10^{-4}$. For oleyl alcohol at $c = 0.11$ μg/cm^2, $Ma = 0.4$, well above the value given in [15] where no-slip behavior is a reasonable approximation. Although the fluid dynamics considered here are different from those investigated by Handler et al. [15], it nevertheless seems likely that a transition to clean surface behavior would not occur in the present system until the oleyl alcohol concentration is reduced by several orders of magnitude. This supposition is predicated on an assumed linear relationship between Ma and c. Further experiments are needed to clarify the actual concentration where the transition between clean and surfactant behavior occurs.

The effect of a surfactant monolayer on the pdfs and statistics of the surface temperature field is now discussed. As the data in Table 2 indicates, for both the high heat flux and the low heat flux cases, the presence of the surfactant monolayer had a small effect on σ. This result contradicts the results of Jarvis [8], who found a significant increase in the fluctuations of the surface temperature time trace when the gas flow rate was high, upon addition of surfactant, and the results of Katsaros and Garrett [10] who showed (at least at intermediate heat fluxes) a significant change in the surface temperature variations of their time traces upon addition of surfactant. The exact cause for this discrepancy is unclear. In both Refs. [8] and [10], the cases where surfactants caused a change in surface temperature fluctuations were cases where a gas flow was imposed. It is possible that their variations in σ were somehow due to this externally imposed flow. Spatial resolution may have also led to the difference. In the present experiments, the spatial resolution was ~0.65 mm in the horizontal direction and 25 μm in the vertical direction. In the work of Jarvis [8] and Katsaros and Garrett [10], measurements were obtained at a depth of 2 mm and the sensor size was always greater than 1 mm. While the spatial resolution reported here is better than that of Jarvis [8] and Katsaros and Garrett [10], and is more than sufficient to resolve the scales in the low flux cases, it should be noted that in the high flux cases, the smallest scales are just barely resolved. Consequently, we conclude that σ probably does not change significantly upon surfactant addition, but that repeating the current high flux experiments at higher resolution and over a larger range of heat flux would be necessary to confirm this conclusion.

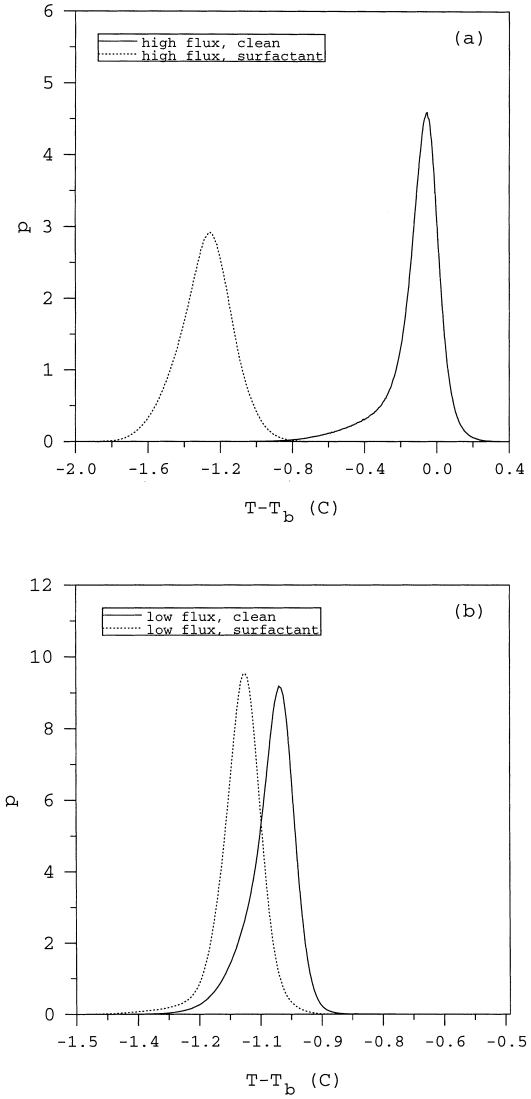

Fig. 9. Probability density function of $T - T_b$ for each of the four experimental conditions. Three lowest spatial frequencies are filtered out of the images prior to obtaining these pdfs. Ensemble average obtained over 119 frames of data. (a) High heat flux cases; (b) low heat flux cases.

For both heat fluxes reported here, the introduction of a monolayer of oleyl alcohol resulted in an increase in the skewness. In the high flux case, the value increased by a factor of 9 and by a factor of 3 in the low flux case. Katsaros and Garrett [10] reported an

increase in skewness when oleyl alcohol was applied, but were not confident in their skewness values.

The increase in skewness, upon application of a surfactant which does not impede evaporation, can be explained in the following way. Variations in temperature at the free surface are due to evaporation. The evaporation process can only result in a decrease in the surface temperature T from the bulk value; evaporation cannot increase T. Hence, T is bounded from above by T_b, and is (effectively) unbounded below. This asymmetry in the bounds for T is most likely the reason why the skewness coefficients are negative for all of the cases.

Without a surfactant monolayer, fluid parcels travel much more rapidly on the surface since there is no monolayer providing a surface elasticity. Hence, they reside on the surface for a short period of time and cannot deviate significantly from T_b, forcing the peak in the pdf to be much closer to T_b. Because the distribution is close to the value of T_b, which it cannot exceed, significant deviations can only occur below the average temperature, causing the distribution to be skewed more to the negative side. When a surfactant monolayer is introduced (at the same heat flux), parcels of fluid on the surface travel more slowly. As a result they reside on the surface for a longer period of time permitting T to drop farther below T_b than for the clean case. Because T is, on the average, farther from T_b, excursions above $\bar{T}$ are not as restricted as for the clean case, and the skewness is not as negative.

This point can be made somewhat clearer if pdfs of the deviation from the bulk temperature T_b, instead of the average temperature $\bar{T}$, are provided. These are presented in Fig. 9. The shape of the pdfs in this figure are identical to those of Fig. 4, the only difference being that the clean and surfactant pdfs are displaced from each other. In Fig. 9(a), the high flux, clean pdf displays a tail which extends into the region $T - T_b > 0$, which is physically not possible. The reason for this is that T_b changes during the course of the experiment. The T_b value reported in Table 1 and used in Fig. 9 is the average value computed over the course of the experiment, allowing for $T - T_b$, to be positive in rare instances. As can be seen, especially for the clean case, the peak of the pdf is very close to $T - T_b = 0$, meaning that many of the fluid parcels do not have sufficient time to cool significantly below the bulk temperature. Consequently, the only variation in temperature which can occur is to the left, making the pdf negatively skewed. For the surfactant case, the majority of the parcels have been cooled significantly beneath T_b, and so most of the warm fluid parcels are not very close to T_b, allowing the pdf to attain a more symmetric shape.

5. Conclusion

Infrared images of the free surface of a body of water undergoing evaporation were obtained. These images were converted into two-dimensional temperature fields of the water surface. Experiments conducted in the presence and absence of a surfactant monolayer, showed that the surfactant monolayer significantly affected the spatial structure and the pdf of the surface temperature field, an observation which has not been made heretofore. This effect was observed when the heat flux was the same in the surfactant and surfactant-free case. The effect of the surfactant monolayer was observed at both low and high heat fluxes. The surfactant monolayer increased the characteristic scale of the structures observed in the infrared imagery and resulted in a more positive skewness coefficient for the probability density function. The rms was only slightly affected by the presence of surfactant. While detailed measurements of the velocity field are necessary in order to ascertain the hydrodynamic mechanism which explains these results, the well known damping characteristics of surfactants seem to account for what was observed.

Acknowledgements

Financial support from the Office of Naval Research, the Naval Research Laboratory, the United States Naval Academy, and the National Research Council is gratefully acknowledged. The authors would like to thank William R. Barger for providing the data presented in Fig. 7.

References

[1] J.C. Berg, A. Acrivos, M. Boudart, Evaporative convection, in: T.B. Drew, J.W. Hoopes, T. Vermeulen, G.R. Cokelet (Eds.), Advances in Chemical Engineering, Academic Press, New York, 1966, pp. 61–124.
[2] E.K. Rideal, On the influence of thin surface films on the evaporation of water, J. Phys. Chem 29 (1925) 1585–1588.
[3] V.K. La Mer (Ed.), Retardation of Evaporation by Monolayers: Transport Processes, Academic Press, New York, 1962.
[4] G.T. Barnes, The effects of monolayers on the evaporation of liquids, Adv. Colloid Interface Sci 25 (1986) 89–200.
[5] U. Navon, J.B. Fenn, Interfacial mass and heat transfer during evaporation. Part I: an experimental technique and some results with a clean water surface, AIChE Journal 17 (1971) 131–136.
[6] U. Navon, J.B. Fenn, Interfacial mass and heat transfer during evaporation. Part II: effect of monomolecular

films on natural convection in water, AIChE Journal 17 (1971) 137–140.
[7] G. Ewing, E.D. McAlister, On the thermal boundary layer of the ocean, Science 131 (1960) 1374–1376.
[8] N.L. Jarvis, The effect of monomolecular films on surface temperature and convective motion at the water/air interface, J. Colloid Sci 17 (1962) 512–522.
[9] N.L. Jarvis, C.O. Timmons, A.W. Zisman, The effect of monomolecular films on the surface temperature of water, in: V.K. La Mer (Ed.), Retardation of Evaporation by Monolayers, Academic Press, New York, 1962, pp. 41–58.
[10] K.B. Katsaros, W.D. Garrett, Effects of organic surface films on evaporation and thermal structure of water in free and forced convection, Int. J. Heat Mass Trans 25 (1982) 1661–1670.
[11] P.P. Lombardini, B. Fiscella, P. Trivero, C. Cappa, W.D. Garrett, Modulation of the spectra of short gravity waves by sea surface films: slick detection and characterization with a microwave probe, Journal of Atmospheric and Oceanic Technology 6 (1989) 882–890.
[12] J.H. Milgram, R.D. Peltzer, O.M. Griffin, Suppression of short sea waves in ship wakes: measurements and observations, JGR 98 (1993) 7103–7114.
[13] R.D. Peltzer, W.D. Garrett, P.M. Smith, A remote-sensing study of a surface ship wake, Int. J. Remote Sensing 8 (1987) 689–704.
[14] W.R. Barger, Unpublished data.
[15] R.A. Handler, G.B. Smith, R.I. Leighton, Vortex interactions with a thermal boundary layer at a surfactant contaminated free surface, in: Proceedings of ASME Fluids Engineering Division Summer Meeting, Washington, DC, 1998.